A NOVEL SAR TARGET DETECTION ALGORITHM BASED ON CONTEXTUAL KNOWLEDGE

Fei Gao[1], Achang Ru[1], Jinping Sun[1, *], and Amir Hussain[2]

[1]School of Electronic and Information Engineering, Beihang University, Beijing, P. R. China

[2]Cognitive Signal-Image and Control Processing Research Laboratory, University of Stirling, Stirling, UK

Abstract—This paper proposes a Synthetic Aperture Radar (SAR) vehicle target detection algorithm based on contextual knowledge. The proposed algorithm firstly obtains the general classification of SAR image with a Markov Random Field (MRF)-based segmentation algorithm; then modifies the prior target presence probability utilizing terrain types, distances to boundary and target aggregation degree; finally gains the detection results using improved Cell Averaging-Constant False Alarm Rate (CA-CFAR). Detections with real SAR image data show that the proposed algorithm can effectively improve target detection rate and reduce false alarms compared with conventional CA-CFAR.

1. INTRODUCTION

SAR is a coherent imaging radar working in microwave band, which has excellent properties and powerful application potential. Countries all over the world have placed great importance on the research of SAR sensors. Rapid development of SAR in recent years has provided higher resolution and fully polarization data. Meanwhile, it makes the fast image interpretation harder [1–3]. A possible solution to this dilemma is describing the characteristics of objects in a reasonable way and combining them with the prior knowledge of targets, which can make full use of information superiority to reduce the uncertainties in detection, and improve the efficiency and reliability of target detection.

Targets of interest in this paper are military vehicles, which may be more likely to be located in fields close to hedges and woodland edges

to provide cover and will often travel in groups. As high resolution SAR provides a wealth of target information and a surveillance capability, vehicles detection with SAR is becoming a hot pot [4, 5].

CFAR (Constant False Alarm Rate) detection has been widely used in target detection of SAR images [6–9]. Literature [10] reviewed the applications of CFAR algorithm with the clutter model of negative exponential, Gamma and K distribution. However many ground clutters may exhibit complicated behaviors, CFAR needs block-by-block estimation of clutter models. It has long been acknowledged that visual context plays an important role in visual perception of object [11, 12]. Consequently, there has been increasing interest in recent years in developing computational models to improve object detection in images by exploiting contextual knowledge [13–22]. Blacknell et al. [23, 24] proposed a contextual knowledge-based target detection algorithm which takes the influence of context to the prior probabilities for the occurrence of targets or clutter into account and validates the algorithm using simulation image. For the simulation image, Blacknell assumed that its edge information was known, but for a real SAR image, it is difficult to get the exact terrain types and edge information.

We propose a SAR image target detection algorithm based on contextual information to solve above problems. Firstly, take a unsupervised classification of real SAR images based on MRF model to get relatively accurate information about the terrain types and edge, which provides the foundation of real SAR images target detection; then we adopt terrain types, distance to boundary and target aggregation degree as impact factors of target presence probability, improve the mathematical model of distance to boundary and target aggregation degree and calculate values of these impact factors; finally obtain the detection results using MAP criterion and CA-CFAR.

2. IMAGE SEGMENTATION BASED ON MRF MODEL

MRF is the most widely used statistical model which has a lot of applications in the fields of image edge detection, segmentation, veins analysis and image recovery [25]. MRF increases the constraints of image process with prior knowledge, combining with Gaussian conditional distribution, MRF provides a convenient method to describe the space-related features of every image pixel in probability. This paper achieves segmentation results utilizing ICM algorithm. Traditional potential function does not work well in SAR image segmentation, so this paper considers the gray value of neighboring pixels, redefines the potential function, and achieves good segmentation results.

2.1. MRF Image Model

An image is composed of finite set S corresponding to the pixels. Therefore, S is essentially a finite discrete system, which is a subset of Z^d, where d is space dimension. Each point of S corresponds to a description operator representing the state of point, the state can be gray, or a marker, or more complex information, it values in a mark-space E.

An image can be treated as a two-dimensional grid point set $S = \{(i,j)|1 \leq i \leq M,\ 1 \leq j \leq N\}$, where M and N are the width and height of image. Mark field $X = \{X_1, X_2, \ldots, X_m\}$ is a random field corresponding to the two-dimensional grid points set S, $X = x$, where $x = \{x_1, x_2, \ldots, x_m\}$ is a configuration of random field X, corresponding to a reality of random field. Each element of S represents the mutual association through a neighborhood system. The neighborhood system of S is defined as follow:

$$N = \{N_i | \forall i \in S\}$$

For a regular grid positions set S, neighborhood of position i is defined as location set whose distance to i is less than $\sqrt{r}$:

$$N_j = \{j \in S \left[\mathrm{dist}\left(\mathrm{pixel}_i, \mathrm{pixel}_j\right)\right]^2 \leq r, \quad i \neq j\}$$

where, dist (A, B) represents the Euclidean distance of A and B, and r is an integer. It should be noted that neighboring pixels in the border location or locations near the border would be less.

Random field X defined on the grid set S with a neighborhood system N becomes a Markov random field when meeting the following two constraints:

(1) Positive definiteness: $P(x) > 0$, $\forall x \in \Omega$;

(2) Markov property: $P(x_i|x_{S/i}) = P(x_i|x_{N_i})$.

where, S/i indicates all positions in grid set S except i, and x_{Ni} represents a set of all neighborhood positions of i. Markov property descries the local characteristics of random field X, direct interactions only exist between the adjacent markers in MRF.

The concept of neighborhood indicates effect distance between pixels, a second-order neighborhood system used in this paper is shown in Figure 1(a). We introduce the concept of group to express effect distance between pixels. Group is a collection of positions, which either contains only an element, or any one in the group is the neighbor of the others. Second-order neighborhood system of single pixel and dual pixel groups is shown in Figure 1(b).
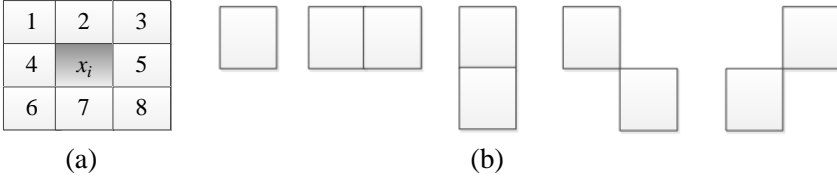
Figure 1. MRF image model. (a) Second-order neighborhood. (b) Single pixel and dual pixel groups.

A conventional potential function is defined as:

$$V(x_i, x_j) = \begin{cases} \beta & x_i = x_j \\ 0 & x_i \neq x_j \end{cases} \tag{1}$$

Segmentation with above function is not ideal as it does not consider the influence of gray value, in the proposed algorithm, we introduced gray value into the potential function, taking full advantage of contexts, the new potential function of gray value is defined as [25]:

$$V'(x_i, x_j) = \begin{cases} \beta & x_i = x_j \\ -\dfrac{\sigma_i^2 \beta}{\left(\sigma_i^2 + k^*(y_i - y_j)^2\right)} & x_i \neq x_j \end{cases} \tag{2}$$

where, σ_i^2 is the variance at position x_i; y_i and y_j are the intensity of observation field at position x_i and x_j; k is the weight of contextual energy $(y_i - y_j)^2$. It can be drawn from formula (2) that the larger gray difference two pixels have, the greater the energy is, and two pixels are less likely classified as the same class.

If the random field configuration obeys Gibbs distribution, we can call this random field GRF, and Gibbs distribution is expressed as:

$$p(x) = Z^{-1} \times e^{-U(x)} \tag{3}$$

where, Z is a normalized constant,

$$Z = \sum_{x \in \Omega} e^{-U(x)} \tag{4}$$

$U(x)$ is a mapping function describing relative intensity of veins, which is the potential sum of all groups in group set C. For isotropic GRF, $U(x)$ can be calculated by the following formula:

$$U(x) = \sum_{\{i\} \in C_1} V_1(x) + \sum_{\{i,j\} \in C_2} V_2(x_i, x_j) + \sum_{\{i,j,k\} \in C_3} V_3(x_i, x_j, x_k) + \dots \tag{5}$$

Only second-order neighborhood systems are considered in this paper, so formula (5) can be simplified:

$$U(x) = \sum_{\{i,j\} \in C_2} V_2(x_i, x_j) \tag{6}$$

MRF is characterized by the local properties of random field, while GRF is described by the entire nature of random field. Harmmersley-Clifford theorem established the equivalence between these two properties. Importance of this theorem is that it provides a simple way to obtain the joint probability. It transforms the interaction between pixels into a priori knowledge.

Process of image segmentation based MRF model is given as follows:

(1) Preprocess the original image, including image smoothing, downsampling, etc.;

(2) Set segmentation parameters (number of categories C, the maximum number of iterations K, weight of context energy k etc.);

(3) Use ICM algorithm for image segmentation: first initialize the state of each pixel, then calculate the local energy per-pixel under different classification marks; finally take the classification mark with the minimum local energy as the current classification mark;

(4) Repeat step (3) K times, get the initial segmentation result;

(5) Use morphological opening and closing operation to remove small dots in the result, then obtain the final segmentation result, take the segmentation boundary as the terrain edge.
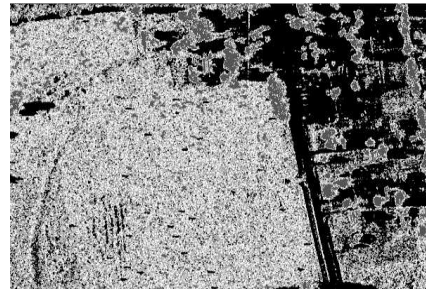
2.2. Segmentation Results

In this paper, we take $C = 3$, $K = 3$, $k = 2.0$, then we divide the original SAR background image shown in Figure 2 into three types, woods areas, grassland areas and shadow areas, as the white areas shown in Figure 3. Woods class and shadows class can be treated as a class in segmentation results because presence probability of targets in these two classes is small, as the white areas shown in Figure 4. We can see from Figure 4 that a part of the grassland areas are divided into woods and shadow areas, reason of this is MRF model is sensitive to veins information, so misclassified cases will appear in grass areas where veins change obviously; grassland area is shown in Figure 5. Image of edge shown in Figure 6 is obtained using results of Figure 4 and Figure 5.
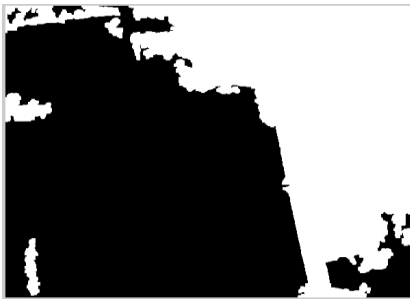
Figures 2–6 show that shadow areas and woods areas can be separated well with the MRF model. Further, we can get the edge information utilizing these two types of classification. Then we can take the contextual knowledge-based target detection utilizing terrain types and edge information.
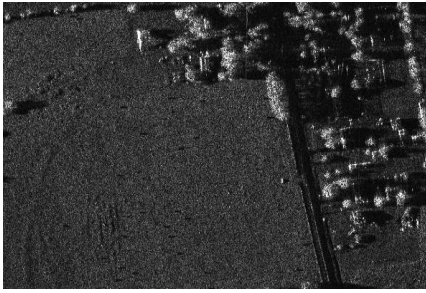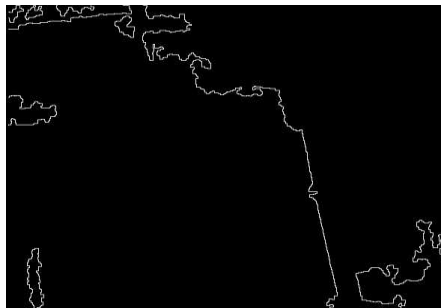
Figure 2. Original SAR image.

Figure 3. Result of MRF segmentation.

Figure 4. Areas of woods and shadows.
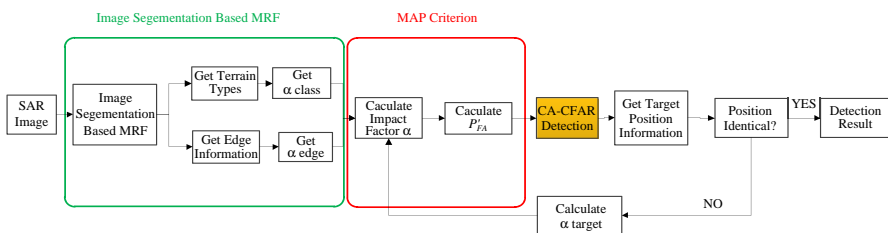

Figure 5. Areas of grassland.

Figure 6. Image of edge.

3. FLOW OF CONTEXTUAL KNOWLEDGE-BASED TARGET DETECTION ALGORITHM

A flow chart of contextual knowledge-based target detection algorithm is shown in Figure 7, and the detailed steps are as follows:

(1) Obtain the general classification of SAR images with MRF-based segmentation algorithm, set α_{class} according to classification results;

(2) Calculate α_{edge} according to edge information obtained in step (1);

(3) Compute total impact factor α without considering α_{target}, calculate class decision threshold of each point with context information, get initial detection results;

(4) Process results of step (3) in morphological method, eliminate the interference portion based on characteristics of detected targets, merge targets;

(5) Calculate α_{target} based on the obtained target positions, update impact factor α, take detection again;

(6) Repeat step (5) until target positions of adjacent results are identical or the maximum number of cycles is reached, then detection process is ended, save the ultimate results.

Figure 7. Flow chart of contextual knowledge-based target detection algorithm.

SAR image classification is difficult and can be achieved by SAR image segmentation, but SAR image segmentation calculation is complicated, and it is difficult to get accurate classification result. High classification accuracy is not required in this paper. A wide range of terrain type can meet the requirements of terrain information. Utilizing contextual information of pixels, a MRF model based segmentation algorithm is adopted to get the initial segmentation result, then morphological opening operation and closing operation are used to merge isolated points and smaller regions. This process reduces the complexity and running time of classification algorithm effectively. Meanwhile, dividing lines between terrain types can be used as edge information directly.

After getting the impact factor α, we can get a new false alarm rate P'_{FA} according to Equation (13), then we can set protection zone and clutter zone like CFAR detector, as classification of image is obtained.

In the process of clutter area calculation, we can select only the clutter points belonging to the same terrain type. This method can prevent the clutter zone from containing different types of terrain, which will result a large deviation. Target detection based on terrain information can estimate model parameters more accurately and obtain more accurate results. But there will be a lot of isolated points and clutter alarms among the target test results because impact of noise and other objects, morphological processing method can be used to get better result: firstly, take morphological closing operation and remove isolated points within the target regions; then filter detection results according to target size to remove interference targets which are too small or too big. The resulting targets are similar to targets to be detected in size.

4. SAR TARGET DETECTION BASED ON CONTEXTUAL KNOWLEDGE

Presence probability of targets may be different in distinct areas of actual SAR images. So we can transform prior knowledge such as geography, surroundings and target characteristics into impact factors of presence probability, which can improve detection rate and reduce false alarms.

4.1. Influence of Presence Probability to Target Detection Rate

MAP criterion is widely used in target detection. Suppose that x is an observation and that $P(t|x)$, $P(b|x)$ are target and clutter posterior probability, then according to of MAP criterion: when $P(t|x) > P(b|x)$, observation x is a target; conversely, x is a clutter.

$$\frac{P(t|x)}{P(b|x)} = \frac{p(x|t) \cdot P(t)}{p(x|b) \cdot P(b)} = \Lambda(x) \cdot \frac{P(t)}{P(b)} \tag{7}$$

where, $p(x|t)$, $p(x|b)$ are probability density functions; $\Lambda(x)$ is likelihood ratio.

In practice, $P(t) \ll 1$, so Equation (7) can be approximated as:

$$\Lambda(x) > \frac{P(b)}{P(t)} = \frac{1 - P(t)}{P(t)} \approx \frac{1}{P(t)} \tag{8}$$

Suppose $x = x_0$, equation $\Lambda(x) = 1/P(t)$ holds, then x_0 is the detection threshold.

In practical applications, considering the influence of prior knowledge, then the presence probability $P(t)$ of target is not fixed.

Assume that impact factor of prior knowledge is α, then the new presence probability $P'(t)$ can be expressed as:

$$P'(t) = \partial \cdot P(t) \tag{9}$$

In reality, distribution of probability density function $p(x|t)$ is complex. $p(x|t)$ can be regarded the same at x_0 and x', namely $p(x_0|t) \approx p(x'|t)$, then we can get:

$$\frac{\Lambda(x_0)}{\Lambda(x')} = \frac{p(x'|b)}{p(x_0|b)} = \partial \tag{10}$$

As to SAR intensity image, clutter obeys negative exponential distribution:

$$p(x|b) = \frac{1}{\mu} \exp\left(-\frac{x}{\mu}\right) \tag{11}$$

By Formulas (10), (11), we can obtain:

$$x' = x_0 - \mu \cdot \ln \partial \tag{12}$$

$$P'_{FA} = \int\limits_{x'}^{\infty} p(x|b)dx = \exp\left(-\frac{x'}{\mu}\right) = \partial P_{FA} \tag{13}$$

Above derivations describe that decision threshold and false alarm probabilities have changed because of the impact of contextual knowledge. By formulas (12) and (13), we can get that detection decision threshold reduces while false alarm probability increases in areas with a large presence probability (impact factor $\alpha > 1$), which will improve the detection rate. On the contrary, detection decision threshold increases while the probability of false alarm reduces in areas with a small presence probability ($\alpha < 1$), so number of false alarms in results is smaller. Compared to CFAR, this process is more in line with the process that human beings detect targets.

Taking the changes of target presence probability into account, false alarm rate P'_{FA} changes α times into the original in the affected areas. Getting value of α and pre-determined false alarm rate P_{FA}, we can obtain a new decision threshold in a way similar to CFAR to get the detection results.

4.2. Impact Factor α

In the process of detection, human will focus on different areas for different interests under a particular scene. For example, areas like the oceans, rivers, lakes, ports will be considered when detecting ships. For the detection of aircrafts, human will focus on airport, or long

straight roads where aircrafts can take off and land. The same with military vehicles, military vehicles may be more likely to be located in fields close to hedges and woodland edges to provide cover and will often travel in groups. All these characteristics are acquired through experience or prior knowledge, which determine the value of impact factors in detection process. We can set the impact factor values according to experience directly, set a greater impact factor in the key areas. Moreover, we can simulate the changes of impact factors with curve.

Against the military vehicles, presence probability of vehicle target is mainly influenced by three factors: terrain type (impact factor α_{class}), target distance to boundary (impact factor α_{edge}) and target aggregation degree (impact factor α_{target}). Assuming that impact factors are independent, the overall impact factor can be given by:

$$\partial = \partial_{class} \cdot \partial_{edge} \cdot \partial_{target} \tag{14}$$

In the following section, detailed discussion of terrain type, target distance to boundary and target aggregation degree will be given.

4.2.1. Impact Factor of Terrain Type (α_{class})

Military vehicles may be more likely located in roads and relatively flat open land, and less likely located in dense woodland, steep mountainous, shadows, etc. When considering the impact of terrain type, we can set the values of impact factors directly according to a prior knowledge.

4.2.2. Impact Factor of Target Distance to Boundary (α_{edge})

When military vehicles located near the edge of woods, presence probability of target gains its maximum at a certain distance from the boundary. Let the distance to boundary be d, then the following formula can be used to simulate impact factor α_{edge}:

$$\partial_{edge} = c \cdot \left(\exp\left\{ -\frac{(d+\varepsilon)^2}{2\sigma_1^2} \right\} - \exp\left\{ -\frac{(d+\varepsilon)^2}{2\sigma_2^2} \right\} \right) \tag{15}$$

Formula (15) shows that the value of impact factor α_{edge} is negative interrelated to distance d. How the α_{edge} changes with distance d is determined by the actual situation and a priori knowledge. Formula (15) is modified based on formula (13) of [24]. The algorithm in [24] used simulated images, where the boundaries were accurate knowable, and targets would not appear at the boundary position; while in reality, it is difficult to obtain accurate boundary information. In this paper, we take broad categories and use morphological method

in the post-process, leading to a certain error between the actual edge and the edge we get, so the value of impact factor cannot be 0 when d is 0. To solve this problem, we added an error correction factor ε, which generally has a length of 1–2 units. In the simulation of α_{edge}, take $c = 3.0$, $\sigma_1 = 5.0$, $\sigma_2 = 1.5$, $\varepsilon = 0.5$, then the simulation of α_{edge} is shown in Figure 8. As can be seen from Figure 8, when the distance is 0, α_{edge} is 0.2, and α_{edge} gains its maximum when d is 2.5. Moreover, α_{edge} decreases as the distance to boundary d increases.

4.2.3. Impact Factor of Target Aggregation Degree (α_{target})

Military vehicles generally move in groups, so if we find some military vehicles in a particular region, it is possible that more targets exist in this region. In addition, we can reduce computation by regarding detected targets as point targets.

Assuming that a target is found at point A and that the distance between B and A is r, according to the interaction between targets, impact factor of point A to point B can be given by:

$$\partial_{target} = M + a \cdot \exp\left\{-\frac{r^2}{l_1^2}\right\} + b \cdot \exp\left\{-\frac{(r-d)^2}{l_2^2}\right\} \qquad (16)$$

By formula (16), we know that when the target distance is small (e.g., $r < 2$), impact factor α_{target} is positively correlated to distance r, but when the distance between targets increases (e.g., $r > 2$), α_{target} has a negative correlation with the distance r. The reason for this phenomenon is that vehicles are less likely to be too close to each other. There is usually a certain distance between two targets, so when the distance is small, the smaller r is, the smaller α_{target} is. Two parts of a target may be regarded as two targets incorrectly in this condition; because the targets usually move or dock in groups, the impact factor α_{target} will be smaller when r is bigger. Take $M = 0.78$, $a = 0.75$,
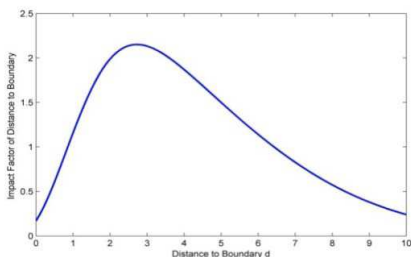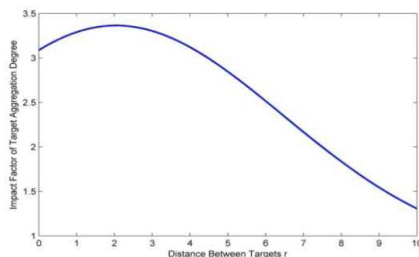

Figure 8. Simulation of α_{edge}.   **Figure 9.** Simulation of α_{target}.

$b = 2$, $l_1 = 5$, $l_2 = 6$, $d = 3$. The simulation of α_{target} can be obtained as shown in Figure 9, when the distance r is 0, α_{target} is 0.2, and α_{target} gains maximum when d is 2. Moreover, α_{target} decreases as the distance to boundary d increases.

Suppose that N targets are detected and that the impacts between these targets are independent, then impact factor of target aggregation degree can be expressed as:

$$\partial_{target} = \partial_{target1} \cdot \partial_{target2}, \ldots, \partial_{targetN} \tag{17}$$

In actual calculations, target locations are unknown, so α_{target} cannot be obtained directly, and we can get it through loop. Take the target detection without α_{target}, calculate α_{target} based on the obtained target positions, then redetect to get new target information. If adjacent target information is inconsistent, repeat above process until adjacent target information is consistent, then the detected targets can be considered as true targets.

5. RESULTS AND ANALYSIS

Experimental image used in this paper is a real MSTAR amplitude image with resolution 0.3 m and size $1784 * 1478$. The known MSTAR public database was collected using the Sandia National Laboratories Twin Otter SAR sensor payload operating at X band with the high resolution of 0.3 m, spotlight mode, HH single polarization. Our interested targets are military vehicles, as shown in Figure 10, and 30 military vehicles are located close to the woods and roads.
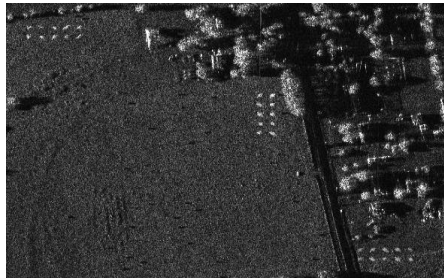
Figure 10. Original image added targets.

In order to reduce the complexity of the count, we transform the targets into point targets and divide the image into blocks. The size of each block is 40×40 and impact factor α approximately constant in the cell blocks.

Taking terrain type into account, set $\alpha_{class} = 1.0$ in grassland areas, $\alpha_{class} = 0.01$ in woods and shadow areas. The distribution of α_{class} is shown in Figure 11(a). Taking $c = 3.0$, $\sigma_1 = 3.0$, $\sigma_2 = 1.5$, $\varepsilon = 3$, distribution of α_{edge} is shown in Figure 11(b). Taking $M = 0.78$, $a = 0.75$, $b = 2$, $l_1 = 5$, $l_2 = 6$, $d = 3$, distribution of α_{target} is shown in Figure 11(c). Considering all context information, we can obtain impact factor α with distribution shown in Figure 11(d). Pixel grey level is shown in Figure 11, and the brighter area indicates higher impact factor and greater presence probability. From the following results we can see that the target presence probability is higher in the woods surroundings, open land, and areas where exists targets. In these regions, impact factor α is also significantly greater than others.

Contextual knowledge-based detection algorithm and CA-CFAR detection algorithm are used in this paper. The detection results of these two detection algorithms are shown in Figures 12–15 in condition of $P_{FA} = 3.17 * 10^{-5}$ and $P_{FA} = 2.87 * 10^{-7}$, respectively.

It can be seen from the above figures that when $P_{FA} = 3.17 * 10^{-5}$, contextual knowledge-based algorithm detects all the 30 targets, only
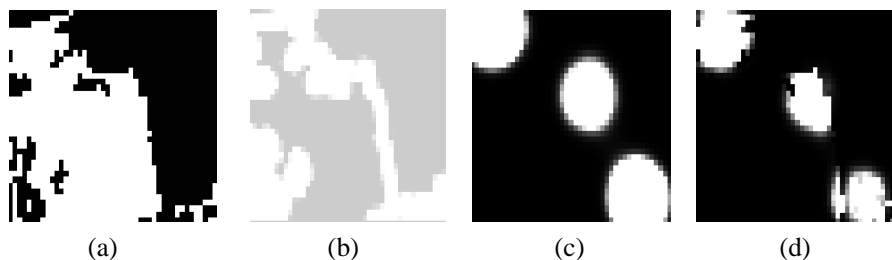

(a)　　　　　　　(b)　　　　　　　(c)　　　　　　　(d)

Figure 11. Distribution of impact factor.

Figure 12. Result of CA-CFAR, when $P_{FA} = 3.17 * 10^{-5}$.

Figure 13. Result of proposed algorithm, when $P_{FA} = 3.17 * 10^{-5}$.

Figure 14. Result of CA-CFAR, when $P_{FA} = 2.87 * 10^{-7}$.

Figure 15. Result of proposed algorithm, when $P_{FA} = 2.87 * 10^{-7}$.

10 false alarms, while the CA-CFAR detects only 24 targets and 16 false alarms; when $P_{FA} = 2.87*10^{-7}$, contextual knowledge-based algorithm and CA-CFAR detects 25 and 24 targets, respectively, but the false alarms of CA-CFAR are 12 more than the contextual knowledge-based algorithm. Therefore, it can be concluded that the contextual knowledge-based algorithm can improve the detection rate effectively and reduce false alarms significantly by taking advantage of a priori knowledge.

To validate the generalization of the proposed algorithm, we adopt images with different backgrounds, and simulation results also illustrate its effectiveness. One of the detection examples is shown in Figure 16.

In Figures 16, (a) is original image added targets; (b)–(c) are results of MRF-based segmentation algorithm; white areas in (b) are woods and shadow, while in (c) are grass, and (d) is the edge image; (e) and (f) represent the detection results of the proposed algorithm and CA-CFAR, respectively, when $P_{FA} = 2.87 * 10^{-7}$. We can obtain from these results that the proposed algorithm is applicable in different conditions.

To analyze the influences of different contextual knowledge, we compare CA-CFAR, contextual knowledge-based algorithm considering one type of context knowledge and the proposed algorithm under different false alarm rates P_{FA}. ROC curves are shown in Figure 17 and Figure 18.

It can be seen from the curves in Figure 17 and Figure 18 that the proposed algorithm has higher detection rates than the other four algorithms, while false alarms in detection results are significantly less. As to detection rate, performance of algorithm only considering distance to boundary is closest to the proposed algorithm, followed
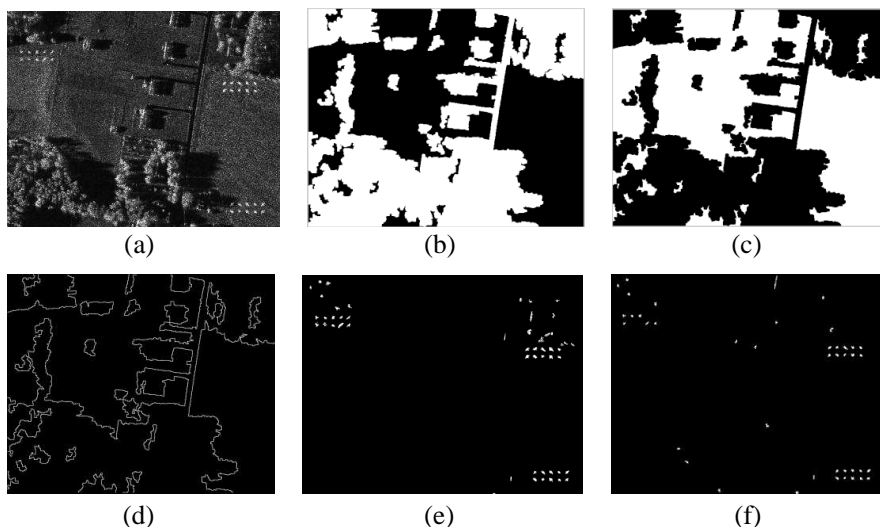
(a)	(b)	(c)
(d)	(e)	(f)

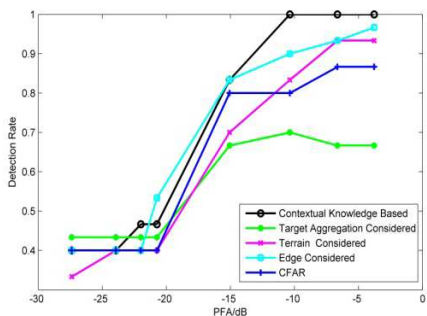**Figure 16.** Results of each step.
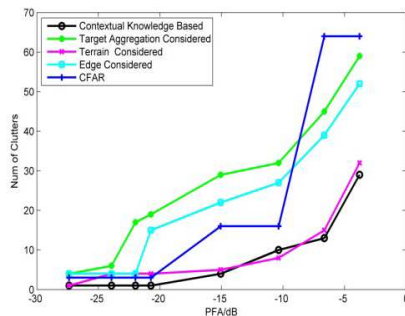

Figure 17. ROC of detection rate.

Figure 18. ROC of false alarms.

by algorithm only considering terrain, and both of these algorithms are better than CA-CFAR, which indicates that the factor of distance to boundary plays an important role in improving detection rate. As to false alarms, performance of algorithm only considering terrain is closest to the proposed algorithm, and the other two algorithms are much worse, which demonstrates that the factor of terrain type can significantly decrease false alarms in detection results. The algorithm only considering target aggregation is the worst of all. The reason is that the factor of target aggregation is heavily dependent on initial

detection results, which will has an adverse influence without a good initial detection result.

In the five detection algorithms, the proposed algorithm is optimal, followed by algorithm only considering terrain type and distance to boundary, respectively. CA-CFAR and algorithm only considering target aggregation do not work well. So we can obtain that the introduction of proper contextual knowledge can reduce the number of false alarms and increase the detection rate.

6. CONCLUSION

Contextual knowledge-based target detection is not only an important trend of artificial intelligence SAR image processing, but also an effective method to reduce the target detection complexity and improve the detection efficiency under complex background. This paper proposes a contextual knowledge-based SAR image vehicle target detection method using given vehicle context knowledge.

Firstly, we propose an unsupervised classification algorithm based on MRF model, utilizing context information of each pixel, then introduce a new potential function, which obtains satisfied classification results and terrain boundaries.

Secondly, give different terrain types corresponding values, then converse the target distance to boundary and the distance between targets to impact factors of target presence probability with suitable mathematical models. Experiments show that these conversion processes can illustrate the influence of context well.

Finally, detect original SAR images according to the MAP criterion. Results show that the proposed algorithm is effective to improve detection efficiency and reduce false alarm and is proved to be an effective vehicle targets detection algorithm in SAR images.

ACKNOWLEDGMENT

REFERENCES

1. Bhanu, B., "Automatic target recognition: State of the art survey," *IEEE Transactions on Aerospace and Electronic Systems*, Vol. 22, No. 4, 364–379, 1984.

2. Tian, B., D.-Y. Zhu, and Z.-D. Zhu, "A novel moving target detection approach for dual-channel SAR system," *Progress In Electromagnetics Research*, Vol. 115, 191–206, 2011.

3. Chiang, C.-Y., Y.-L. Chang, and K.-S. Chen, "SAR image simulation with application to target recognition," *Progress In Electromagnetics Research*, Vol. 119, 35–57, 2011.

4. Szottka, I. and M. Butenuth, "Tracking multiple vehicles in airborne image sequences of complex urban environments," *2011 Joint Urban Remote Sensing Event*, 13–16, Munich, 2011.

5. Gerhardinger, A., D. Ehrlich, and M. Pesaresi, "Vehicles detection from very high resolution satellite imagery," *International Archives of Photogrammetry and Remote Sensing*, Vol. 36, Part 3/W24, 83–88, 2005.

6. Di Bisceglie, M. and C. Galdi, "CFAR detection of extended objects in high-resolution SAR images," *IEEE Transactions on Geoscience and Remote Sensing*, Vol. 43, No. 4, 833–843, 2005.

7. Gao, G., "A Parzen-window-kernel-based CFAR algorithm for ship detection in SAR images," *IEEE Transactions on Geoscience and Remote Sensing Letters*, Vol. 8, No. 3, 557–561, 2011.

8. Habib, M. A., M. Barkat, B. Aissa, and T. A. Denidni, "CA-CFAR detection performance of radar targets embedded in 'non-centered Chi-2 Gamma' clutter," *Progress In Electromagnetics Research*, Vol. 88, 135–148, 2008.

9. Cui, Y., G. Zhou, J. Yang, and Y. Yamaguchi, "On the iterative censoring for target detection in SAR images," *IEEE Transactions on Geoscience and Remote Sensing Letters*, Vol. 8, No. 4, 641–645, 2011.

10. Oliver, C. J. and S. Quegan, *Understanding Synthetic Aperture Radar Images,* Artech House, Norwood, MA, 1998.

11. Bar, M. and S. Ullman, "Spatial context in recognition," *Perception*, Vol. 25, No. 3, 343–352, 1993.

12. Biederman, I., R. J. Mezzanotte, and J. C. Rabinowitz, "Scene perception: Detecting and judging objects undergoing relational violations," *Cognitive Psychology*, Vol. 14, 143–177, 1982.

13. Carbonetto, P., N. de Freitas, and K. Barnard, "A statistical model for general contextual object recognition," *Proc. European Conf. Computer Vision*, Vol. 3021, 350–362, 2004.

14. Divvala, S. K., D. Hoiem, J. H. Hays, A. A. Efros, and M. Hebert, "An empirical study of context in object detection," *Proc. IEEE Conf. Computer Vision and Pattern Recognition*, 2009.

15. Galleguillos, C. and S. Belongie, "Context based object

categorization: A critical survey," *Computer Vision and Image Understanding*, Vol. 114, No. 6, 712–722, 2010.

16. Galleguillos, C., A. Rabinovich, and S. Belongie, "Object categorization using co-occurrence, location and appearance," *Proc. IEEE Conf. Computer Vision and Pattern Recognition*, 1–8, 2008.

17. Tian, B., D.-Y. Zhu, and Z.-D. Zhu, "A novel moving target detection approach for dual-channel SAR system," *Progress In Electromagnetics Research*, Vol. 115, 191–206, 2011.

18. Kumar, S. and M. Hebert, "A hierarchical field framework for unified context-based classification," *IEEE 10th International Conference on Computer Vision*, 1284–1291, 2005.

19. Chang, Y.-L., C.-Y. Chiang, and K.-S. Chen, "SAR image simulation with application to target recognition," *Progress In Electromagnetics Research*, Vol. 119, 35–57, 2011.

20. Rabinovich, A., A. Vedaldi, C. Galleguillos, E. Wiewiora, and S. Belongie, "Objects in context," *IEEE 11th International Conference on Computer Vision*, 1–8, 2007.

21. Diao, W.-H., X. Mao, H.-C. Zheng, Y.-L. Xue, and V. Gui, "Image sequence measures for automatic target tracking," *Progress In Electromagnetics Research*, Vol. 130, 447–472, 2012.

22. Zhang, X., J. Qin, and G. Li, "SAR target classification using bayesian compressive sensing with scattering centers features," *Progress In Electromagnetics Research*, Vol. 136, 385–407, 2013.

23. Blacknell, D., S. Arini Nicholas, and I. McConnell, "SAR image understanding using contextual information," *Proc. SPIE, SAR Image Analysis, Modeling, and Techniques IV*, Vol. 4543, 73284, 2001.

24. Blacknell, D., "Contextual information in SAR target detection," *IEEE Proceedings: Radar, Sonar and Navigation*, Vol. 148, No. 1, 41–47, 2001.

25. Noda, H., M. N. Shirazi, and E. Kawaguchi, "MRF-based texture segmentation using wavelet decomposed images," *Pattern Recognition*, Vol. 35, No. 4, 771–782, 2002.